JEM-2010 analytical transmission electron microscope was used. Detailed TEM observations of these and other samples are reported elsewhere (N. Miyajima *et al.*, in preparation).
11. E. Ito and Y. Matsui, *Earth Planet. Sci. Lett.* **38**, 443 (1978); T. Yagi, H. K. Mao, P. M. Bell, *Phys. Chem. Miner.* **3**, 97 (1978).
12. We often observe stishovite even for enstatite ($MgSiO_3$) heated by the YAG laser, which is known to transform to the single phase of perovskite. It is also observed in our multi-anvil experiments, in which the heating duration is 1 to 2 min at ~1800 K, but it usually disappears by heating for 30 min or more at the same temperature.
13. The x-ray diffraction lines of the garnet are broad compared with those of the other phases, indicating the presence of unrelaxed stress. The unit cell parameter of the recovered garnet is the same as that of the starting material within experimental uncertainty. In addition, the garnet has not been observed by TEM, probably because the low-temperature part of the sample, which had been adjacent to diamonds, was removed during ion-thinning. From these observations, we believe that the garnet observed after heating is residual starting material.
14. H. K. Mao *et al.*, *J. Geophys. Res.* **96**, 8069 (1991); N. Funamori, T. Yagi, T. Uchida, W. Utsumi, *Proc. 14th AIRAPT Conf.*, 791 (1994).
15. L. G. Liu, *Earth Planet. Sci. Lett.* **31**, 200 (1976); E. Ito and Y. Matsui, in *High-Pressure Research: Applications in Geophysics*, M. H. Manghnani and S. Akimoto, Eds. (Academic Press, New York, 1977), pp. 193–208.
16. K. Leinenweber, W. Utsumi, Y. Tsuchida, T. Yagi, K. Kurita, *Phys. Chem. Miner.* **18**, 244 (1991).
17. R. D. Shannon and C. T. Prewitt, *Acta. Crystallogr.* **B26**, 925 (1969).
18. N. L. Ross, J. Ko, C. T. Prewitt, *Phys. Chem. Miner.* **16**, 621 (1989).
19. K. Leinenweber, Y. Wang, T. Yagi, H. Yusa, *Am. Mineral.* **79**, 197 (1994).
20. The orthorhombic perovskite with $Ca_3Al_2Si_3O_{12}$ composition transforms to amorphous phase on release of pressure [H. Yusa *et al.*, *Phys. Earth Planet. Inter.* **92**, 25 (1995)]. Although the *t* value of $Ca_3Al_2Si_3O_{12}$ (0.88) is smaller than that of $Ca_4Si_4O_{12}$ (0.94), it is still very large because of the large radius of Ca^{2+}.
21. J. Ko and C. T. Prewitt, *Phys. Chem. Miner.* **15**, 355 (1988).
22. T. Irifune, *Nature* **370**, 131 (1994).
23. B. O'Neill and R. Jeanloz, *Geophys. Res. Lett.* **17**, 1477 (1990).
24. D. L. Heinz and R. Jeanloz, *J. Geophys. Res.* **92**, 11437 (1987).
25. We thank O. Shimomura, T. Kikegawa, K. Aoki, H. Fujihisa, H. Yamawaki, T. Kondo, T. Uchida, and M. Yamakata for support of the experiments and R. Jeanloz, M. Akaogi, and C. T. Prewitt for helpful comments. The garnet sample was provided by T. Watanabe and A. Agashev. X-ray experiments were carried out at KEK (96S02). N.F. and N.M. were supported by Research Fellowships of the Japan Society for the Promotion of Science for Young Scientists.

30 July 1996; accepted 10 December 1996

An $Fe^{IV}_2O_2$ Diamond Core Structure for the Key Intermediate Q of Methane Monooxygenase

Lijin Shu, Jeremy C. Nesheim, Karl Kauffmann, Eckard Münck, John D. Lipscomb, Lawrence Que Jr.*

A new paradigm for oxygen activation is required for enzymes such as methane monooxygenase (MMO), for which catalysis depends on a nonheme diiron center instead of the more familiar Fe-porphyrin cofactor. On the basis of precedents from synthetic diiron complexes, a high-valent $Fe_2(\mu\text{-}O)_2$ diamond core has been proposed as the key oxidizing species for MMO and other nonheme diiron enzymes such as ribonucleotide reductase and fatty acid desaturase. The presence of a single short Fe–O bond (1.77 angstroms) per Fe atom and an Fe–Fe distance of 2.46 angstroms in MMO reaction intermediate Q, obtained from extended x-ray absorption fine structure and Mössbauer analysis, provides spectroscopic evidence that the diiron center in Q has an $Fe^{IV}_2O_2$ diamond core.

The MMO enzyme system found in methanotrophic bacteria initiates the oxidation of methane (*1*, *2*), thereby preventing the atmospheric egress of nearly 1 billion tons of this greenhouse gas annually. MMO catalyzes the difficult oxidation of methane (CH_4) to methanol (CH_3OH) with incorporation of one oxygen atom from O_2. The soluble MMO system consists of three separate protein components termed the hydroxylase (MMOH), reductase (MMOR), and component B (MMOB) (*3*, *4*). The crystal structures of MMOH have revealed a nonheme diiron active site (*5*–*7*) where oxygen activation and substrate oxidation occur (*4*). Transient kinetic analysis of a single-turnover reaction has revealed at least five and probably six intermediates in the catalytic cycle, among which intermediate Q is the key oxidizing species (*8*–*11*). The Mössbauer properties of Q indicate an exchange-coupled high-valent $Fe^{IV}Fe^{IV}$ cluster. The Fe^{IV} oxidation state has been assigned on the basis of the large decrease in isomer shift from $\delta = 0.50$ mm s^{-1} for $Fe^{III}Fe^{III}$ MMOH to $\delta = 0.17$ mm s^{-1} for Q (*12*); the latter value is comparable to the δ values for well-characterized Fe^{IV} complexes (*13*, *14*). To date, no high-valent intermediate of any metallooxygenase has been structurally characterized. Here, we report extended x-ray absorption fine structure (EXAFS) studies of *Methylosinus trichosporium* OB3b MMOH intermediate Q that provide spectroscopic evidence that an enzyme uses an $Fe_2(\mu\text{-}O)_2$ diamond core for alkane oxidation (*15*).

A rapid freeze-quench technique allowed us to trap Q in the optimal time domain after mixing $Fe^{II}Fe^{II}$ MMOH with 100% O_2-saturated buffer in the presence of two equivalents of MMOB (*8*, *9*, *12*). The samples were analyzed by Mössbauer spectroscopy to provide an independent quantitation of the reaction cycle intermediates in the samples before and after the x-irradiation inherent in the EXAFS experiment. Figure 1 shows a 4.2 K Mössbauer spectrum of Q sample 1 and the corresponding features that make up this spectrum. The progressive decrease in isomer shift δ upon passage through successive reaction cycle intermediates $Fe^{II}Fe^{II}$ MMOH, P (*16*), and Q indicates the increasing oxidation state of the two Fe sites. The Mössbauer-determined compositions of the two freeze-quenched samples 1 and 2 are listed in Table 1. As indicated, intermediate Q represented substantial fractions of each sample, 61% and 44%, respectively; these percentages were the same before and after irradiation.

The *R*-space EXAFS spectra of four MMOH samples (*17*) have features that correspond to the distances from each Fe site to surrounding atoms (Fig. 2). For example, the $Fe^{II}Fe^{II}$ MMOH sample shows one prominent feature at $R \sim 2.1$ Å (Fig.

Table 1. Compositions of freeze-quenched EXAFS samples of MMOH intermediate Q determined by Mössbauer spectroscopy. An optimal time window from 100 to 320 ms, determined by stopped-flow spectroscopy at 17°C, was used to quench a single-turnover reaction and trap intermediate Q according to the experimental procedure reported previously (*8*, *9*, *12*). Sample 1 was trapped at 150 ms and sample 2 was trapped at 300 ms, allowing us to study two samples with different concentrations of Q for comparison of their EXAFS feature intensities.

Sample	$Fe^{II}Fe^{II}$ form	Intermediate P	Intermediate Q	$Fe^{III}Fe^{III}$ form
1	27%	5%	61%	7%
2	33%	5%	44%	18%*

*Samples 1 and 2 both have a contribution from $Fe^{III}Fe^{III}$ MMOH. The spectrum of sample 2 revealed an additional species with parameters similar to those of the oxo-bridged $Fe^{III}Fe^{III}$ cluster of ribonucleotide reductase. We have seen this component in various samples prepared to trap intermediates of the MMOH cycle.

L. Shu and L. Que Jr., Department of Chemistry and Center for Metals in Biocatalysis, University of Minnesota, Minneapolis, MN 55455, USA.
J. C. Nesheim and J. D. Lipscomb, Department of Biochemistry, Medical School, and Center for Metals in Biocatalysis, University of Minnesota, Minneapolis, MN 55455, USA.
K. Kauffmann and E. Münck, Department of Chemistry, Carnegie Mellon University, Pittsburgh, PA 15213, USA.
*To whom correspondence should be addressed. E-mail: QUE@chem.umn.edu

2A) that represents the first coordination sphere around the iron sites. This peak is best fit by a shell of 0.5 O/N atom per Fe at 2.02 Å and 4 O/N atoms at 2.20 Å (Table 2); this result is consistent with the presence of four carboxylates, two histidines, and two solvent molecules ligated to the diiron center, as revealed by the crystal structure of the $Fe^{II}Fe^{II}$ MMOH from *Methylococcus capsulatus* (Bath) (6). The feature at $R \sim 3.4$ Å corresponds to an Fe–Fe distance of 3.43 Å (Table 2), which is slightly longer than the 3.28 Å distance deduced from x-ray crystallography (6). This Fe-Fe interaction could not be discerned in the EXAFS analysis of $Fe^{II}Fe^{II}$ MMOH from *M. capsulatus* (Bath) (18).

Figure 2D shows the *R*-space spectrum of a sample labeled "decayed Q" in which intermediate Q had been formed and then allowed to decay completely by standing at room temperature for 10 min, as indicated by the loss of its characteristic yellow color. The *R*-space spectrum resembles that previously reported for $Fe^{III}Fe^{III}$ MMOH (19) and can be simulated with similar parameters (Table 2); in particular, there are two different Fe–Fe distances, 3.03 and 3.32 Å, that correspond to the presence of two populations of diiron center with different core structures (19).

In contrast to the $Fe^{II}Fe^{II}$ MMOH and decayed Q samples, the two Q samples show three prominent peaks at $R \sim 1.5$, 2, and 2.5 Å in their *R*-space spectra (Fig. 2, B and C). The 2 Å feature corresponds to a shell of 4 O/N atoms at ~2.05 Å (Table 2), and its large Debye-Waller factor arises from the wide range of Fe–ligand bond lengths expected for a sample consisting of several different species. The new features at $R \sim 1.5$ and 2.5 Å originate from an O/N atom at 1.77 Å and an Fe atom at 2.46 Å (Table 2). The intensities of these new features in the two Q samples and the partial occupancies derived from the fits are in agreement with the amount of Q determined by Mössbauer spectroscopy.

The pre-edge region of an x-ray absorption spectrum provides information that complements the EXAFS analysis, as the integrated area of the pre-edge $1s \rightarrow 3d$ transition is sensitive to the centrosymmet-

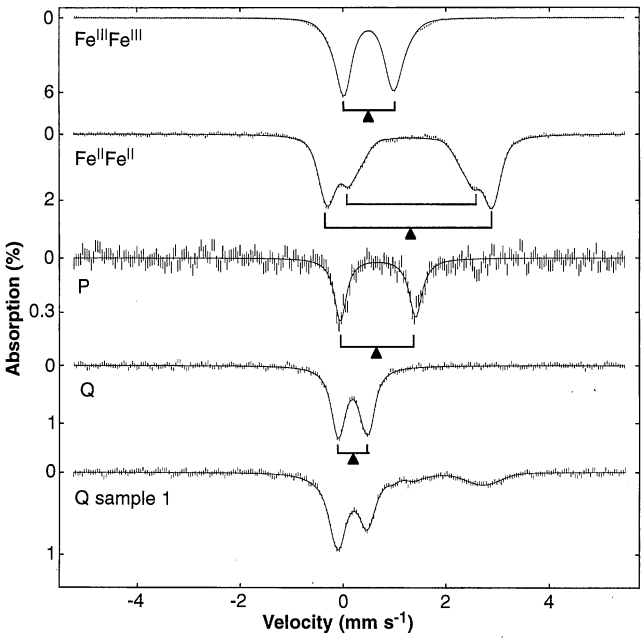

Fig. 1. Mössbauer spectra of MMOH from *Methylosinus trichosporium* OB3b recorded at 4.2 K. Shown are representative spectra of $Fe^{III}Fe^{III}$ MMOH (δ = 0.50 mm s^{-1}), $Fe^{II}Fe^{II}$ MMOH (δ = 1.30 mm s^{-1}), and transient intermediates P ($Fe^{III}Fe^{III}$, δ = 0.67 mm s^{-1}) and Q ($Fe^{IV}Fe^{IV}$, δ = 0.17 mm s^{-1}), as well as the spectrum of Q sample 1 used for EXAFS studies. Quadrupole doublets are indicated by brackets; isomer shifts δ are marked by filled triangles. The solid line drawn through the spectrum of sample 1 is a superposition of computed spectra for the $Fe^{II}Fe^{II}$ and $Fe^{III}Fe^{III}$ forms, P, and Q using fractions listed in Table 1.

Table 2. X-ray absorption spectroscopic data analysis for samples in the catalytic pathway of MMOH. The diiron cluster concentration in Q samples 1 and 2 was ~0.5 mM, whereas that for the $Fe^{II}Fe^{II}$ and decayed Q samples was ~1.5 mM with 25% (v/v) glycerol. The latter sample was bubbled with O_2 to ensure complete reaction. The buffer for all experiments was 100 mM MOPS (pH 7.7). The ranges for EXAFS data fitting and Fourier transform were as follows: 1.35 to 4.05 Å and 2 to 12 $Å^{-1}$ ($Fe^{II}Fe^{II}$ MMOH); 1.25 to 3.15 Å and 2 to 11 $Å^{-1}$ (Q samples 1 and 2); and 1.35 to 3.55 Å and 2 to 14 $Å^{-1}$ (decayed Q). Values in parentheses represent σ^2, the Debye-Waller factors, which reflect the extent of disorder (static and dynamic) within the shells. The negative values for the short Fe-O shells are typical of short iron-oxo bonds and merely reflect the weaker and longer bonds of the $Fe(acac)_3$ standard (acac, acetylacetonate) (40).

Sample	Fit of EXAFS region	Pre-edge area (units)
$Fe^{II}Fe^{II}$ MMOH	4 O/N at 2.20 Å (0.0067) 0.5 O/N at 2.02 Å (0.0039) 1 Fe at 3.43 Å (0.0062)	10 ± 1
Sample 1 (61% Q)	4 O/N at 2.05 Å (0.0115) 0.6 O/N at 1.77 Å (−0.0003) 0.6 Fe at 2.46 Å (0.0086)*	22 ± 1
Sample 2 (44% Q)†	4 O/N at 2.03 Å (0.0063) 0.5 O/N at 1.78 Å (−0.0039) 0.5 Fe at 2.47 Å (0.0058)*	18 ± 1
Decayed Q	5 O/N at 2.01 Å (0.0059) 0.6 Fe at 3.03 Å (0.0015) 0.4 Fe at 3.32 Å (0.0061)	14 ± 1

*Attempts to fit this 2.46 Å shell with low atomic number atoms gave rise to unacceptable fits. †The 3.4 Å feature in the spectrum (Fig. 2C) of this sample was not included in the window used for the fit. When the window was extended to include this feature, it represented 0.5 Fe at 3.42 Å, which we attribute to contributions from the $Fe^{II}Fe^{II}$ and $Fe^{III}Fe^{III}$ forms of MMOH.

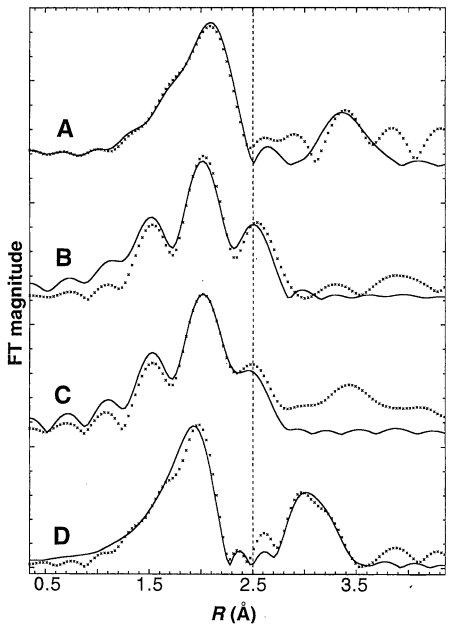

Fig. 2. Fourier-transformed (FT) EXAFS experimental data (dotted line) and fits (solid line; see Table 2) of (**A**) $Fe^{II}Fe^{II}$ MMOH, (**B**) Q sample 1 (61% Q, trapped at 150 ms), (**C**) Q sample 2 (44% Q, trapped at 300 ms), and (**D**) decayed Q. The values of *R* on the *x* axis have been arbitrarily incremented by 0.35 Å, a typical phase shift, to provide a more realistic estimate of the metal–scatterer distances. Only shells with $R < 3$ Å were considered for the fits for Q samples 1 and 2. The vertical dashed line drawn through all the spectra highlights the presence of the 2.5 Å feature characteristic of intermediate Q.

ric nature and the coordination number of the metal site (*20, 21*). The $Fe^{II}Fe^{II}$ MMOH and decayed Q samples have pre-edge areas of 10 and 14 units, respectively (Table 2); these values fall in the reported range for five-coordinate iron sites (*20, 21*). In contrast, each Fe^{IV} site of intermediate Q in samples 1 and 2 has a pre-edge area of 28 units (*22*). This large value implies that the Fe^{IV} centers in Q have a highly distorted geometry and are likely to have a coordination number no greater than 5. The highly distorted geometry and the consequent large pre-edge area observed here result from the presence of a short Fe–O bond (1.77 Å), analogous to observations for diiron complexes having an oxo bridge (*20*).

Our EXAFS analysis of intermediate Q thus shows a species with two structural features not found in either $Fe^{II}Fe^{II}$ or $Fe^{III}Fe^{III}$ MMOH (*18, 19*): a single 1.77 Å Fe–O bond per Fe atom and a 2.46 Å separation between the two Fe^{IV} ions. A length of 1.77 Å is too long to be associated with a terminal Fe^{IV}=O bond, as found in high-valent iron-oxo porphyrins and heme peroxidase compounds I and II (1.60 to 1.66 Å) (*23*), but is consistent with an Fe–μ-O bond of a (μ-oxo)diiron unit (1.74 to 1.82 Å) (*24*). A short Fe–Fe separation of ~2.5 Å has not yet been observed for any diiron-oxo protein, although Fe–Fe distances of 2.7 Å are common for Fe-S proteins (*25*). Such short distances can only be enforced by the presence of two single-atom bridges forming a diamond-shaped core. Precedents of such a $M_2(\mu\text{-}O)_2$ (M = metal) diamond core have been found for synthetic complexes (*26–30*) as well as for the O_2-evolving complex of photosystem II (*31, 32*), where the metal-metal distances range from 2.5 to 2.9 Å.

The sole crystallographically characterized example of a synthetic $Fe_2(\mu\text{-}O)_2$ diamond core, $[Fe^{III}_2(\mu\text{-}O)_2(6\text{-}Me_3\text{-}TPA)](ClO_4)_2$ [6-Me_3-TPA = tris(6-methylpyridyl-2-methyl)amine], has a centrosymmetric rhomb with Fe–μ-O distances of 1.84 and 1.92 Å and an Fe–Fe distance of 2.7 Å (*27*). Given the EXAFS analysis and the Mössbauer evidence for nearly identical Fe^{IV} sites (*12*), we propose that MMOH intermediate Q has an analogous $Fe^{IV}_2O_2$ diamond core structure (Scheme 1). Consistent with its higher valent state, the short Fe–O bonds (1.77 Å) for Q are shorter than those of the synthetic compound with an $Fe^{III}_2(\mu\text{-}O)_2$ core (*27*) but are comparable to those of a complex with an $Fe^{III}Fe^{IV}(\mu\text{-}O)_2$ core (*28*). The 2.46 Å Fe–Fe distance for Q is, however, shorter than those found in these model complexes (2.7 to 2.9 Å). In synthetic Mn_2O_2 complexes, the Mn–Mn distance can be shortened by ~0.1 Å with the introduction of an additional carboxylate bridge (*33*). This observation prompts us to propose the presence of such a bridge for Q. Indeed, a carboxylate bridge (Glu^{144}) is a common feature in all of the $Fe^{II}Fe^{II}$ and $Fe^{III}Fe^{III}$ MMOH crystal structures (*5–7*). This carboxylate bridge may serve to hold the diiron unit together as it proceeds through the catalytic cycle (*1*).

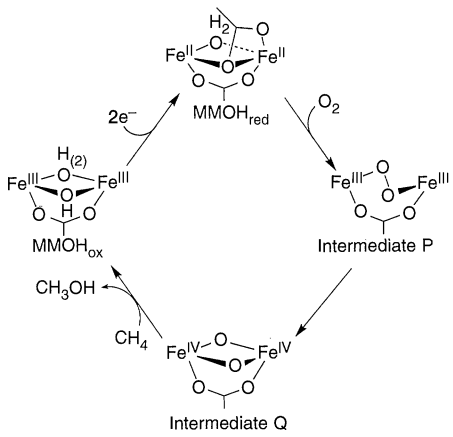

Scheme 1. Diiron core structures of key species in the catalytic cycle of MMOH.

Scheme 1 illustrates the proposed structural changes in the diiron unit during catalysis. The $Fe_2(\mu\text{-}O)_2$ diamond core has been proposed to be the key high-valent species in the oxidation of substrate in nonheme diiron enzymes on the basis of structural, spectroscopic, and reactivity studies of synthetic diiron complexes (*15*). Our combined Mössbauer-EXAFS investigation provides experimental evidence that such a diamond core participates in the MMO reaction cycle. This core can be readily attained by homolysis of the O–O bond in its precursor P (*34*), which, from a comparison with model complexes (*35–37*), is likely to be a (μ-1,2-peroxo)diiron(III) species (Scheme 1).

The $Fe^{IV}_2(\mu\text{-}O)_2$ diamond core addresses how nonheme diiron active sites store the oxidizing equivalents. In cytochrome P-450 (*38*), one oxidizing equivalent is proposed to be stored on the iron center and another on the porphyrin ligand, forming a short-lived Fe^{IV}=O porphyrin radical species, which is equivalent to heme peroxidase compound I (*39*). For MMO, the role of the porphyrin is assumed by the second iron, and each iron site serves to store one oxidizing equivalent by forming an $Fe^{IV}Fe^{IV}$ species (*12*). The EXAFS-derived dimensions of the $Fe^{IV}_2(\mu\text{-}O)_2$ core indicate that each iron has one short (~1.77 Å) and one long (~2.05 Å) Fe–μ-O bond, which suggests that this structure may be viewed as a head-to-tail dimer of Fe^{IV}=O units (Scheme 2). This dimerization may serve to stabilize the high-valent iron-oxo moiety, thereby allowing its observation and characterization in MMO. Although MMOH intermediate Q appears to be functionally equivalent to the reactive species of cytochrome P-450, the structural divergence of the key reactive species revealed here offers the possibility that a novel manifestation of the chemistry of

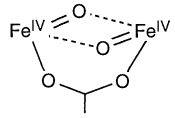

Scheme 2.

highly activated oxygen in biology will emerge from continuing studies.

The spectroscopic studies described here provide direct experimental evidence for the participation of an $Fe_2(\mu\text{-}O)_2$ diamond core in the catalytic cycle of MMO. This precedent lends credence to the hypothesis that such $Fe_2(\mu\text{-}O)_2$ cores participate in the redox cycles of related nonheme diiron enzymes such as ribonucleotide reductase, fatty acid desaturases, and membrane alkane hydroxylases (*1, 15*).

REFERENCES AND NOTES

1. B. J. Wallar and J. D. Lipscomb, *Chem. Rev.* **96**, 2625 (1996).
2. K. E. Liu and S. J. Lippard, *Adv. Inorg. Chem.* **42**, 263 (1995).
3. J. Colby and H. Dalton, *Biochem. J.* **171**, 461 (1978).
4. B. G. Fox, W. A. Froland, J. E. Dege, J. D. Lipscomb, *J. Biol. Chem.* **264**, 10023 (1989).
5. A. C. Rosenzweig, C. A. Frederick, S. J. Lippard, P. Nordlund, *Nature* **366**, 537 (1993).
6. A. C. Rosenzweig, P. Nordlund, P. M. Takahara, C. A. Frederick, S. J. Lippard, *Chem. Biol.* **2**, 409 (1995).
7. N. Elango *et al.*, *Protein Sci.*, in press.
8. S.-K. Lee, J. C. Nesheim, J. D. Lipscomb, *J. Biol. Chem.* **268**, 21569 (1993).
9. Y. Liu, J. C. Nesheim, S.-K. Lee, J. D. Lipscomb, *ibid.* **270**, 24662 (1995).
10. K. E. Liu *et al.*, *J. Am. Chem. Soc.* **117**, 10174 (1995).
11. J. C. Nesheim and J. D. Lipscomb, *Biochemistry* **35**, 10240 (1996).
12. S.-K. Lee, B. G. Fox, W. A. Froland, J. D. Lipscomb, E. Münck, *J. Am. Chem. Soc.* **115**, 6450 (1993).
13. Y. Dong, L. Que Jr., K. Kauffmann, E. Münck, *ibid.* **117**, 11377 (1995).
14. T. J. Collins, K. L. Kostka, E. Münck, E. S. Uffelman, *ibid.* **112**, 5637 (1990).
15. L. Que Jr. and Y. Dong, *Acc. Chem. Res.* **29**, 190 (1996).
16. Intermediate P has been proposed to have a (μ-1,2-peroxo)diiron(III) core on the basis of Mössbauer and resonance Raman studies (*34*).
17. X-ray absorption spectra were collected at Beamline X9B of the National Synchrotron Light Source (NSLS) at Brookhaven National Laboratory. The details of data collection and the procedure of EXAFS data extraction and analysis have been presented (*40*) [L. Shu *et al.*, *Biochemistry* **34**, 6649 (1995)].
18. J. G. DeWitt *et al.*, *Inorg. Chem.* **34**, 2505 (1995).
19. L. Shu, Y. Liu, J. D. Lipscomb, L. Que Jr., *J. Biol. Inorg. Chem.* **1**, 297 (1996).
20. A. L. Roe *et al.*, *J. Am. Chem. Soc.* **106**, 1676 (1984).
21. C. R. Randall *et al.*, *Inorg. Chem.* **34**, 1036 (1995).
22. This value for the pre-edge area of Q was obtained by subtracting out the contributions of the $Fe^{II}Fe^{II}$

and $Fe^{III}Fe^{III}$ forms of MMOH, based on their Mössbauer-determined percentages in the freeze-quenched samples. For sample 1, the pre-edge area of Q = {22 units − [(27%)(10 units)] − [(12%)(14 units)]}/61% = 29 units. For sample 2, the pre-edge area of Q = {18 units − [(33%)(10 units)] − [(23%)(14 units)]}/44% = 26 units.
23. J. E. Penner-Hahn *et al.*, *J. Am. Chem. Soc.* **108**, 7819 (1986).
24. D. M. Kurtz Jr., *Chem. Rev.* **90**, 585 (1990).
25. J. M. Berg and R. H. Holm, in *Iron-Sulfur Proteins*, T. G. Spiro, Ed. (Wiley, New York, 1982), pp. 3–66.
26. V. L. Pecoraro, M. J. Baldwin, A. Gelasco, *Chem. Rev.* **94**, 807 (1994).
27. Y. Zang, Y. Dong, L. Que Jr., K. Kauffmann, E. Münck, *J. Am. Chem. Soc.* **117**, 1169 (1995).
28. Y. Dong *et al.*, *ibid.*, p. 2778.
29. S. Mahapatra *et al.*, *ibid.*, p. 8865.
30. J. A. Halfen *et al.*, *Science* **271**, 1397 (1996).
31. V. K. Yachandra *et al.*, *ibid.* **260**, 675 (1993).
32. P. J. Riggs-Gelasco, R. Mei, C. F. Yocum, J. E. Penner-Hahn, *J. Am. Chem. Soc.* **118**, 2387 (1996).
33. K. R. Reddy, M. V. Rajasekharan, S. Padhye, F. Dahan, J.-P. Tuchagues, *Inorg. Chem.* **33**, 428 (1994).
34. K. E. Liu *et al.*, *J. Am. Chem. Soc.* **117**, 4997 (1995).
35. T. Ookubo *et al.*, *ibid.* **118**, 701 (1996).
36. Y. Dong, S. Yan, V. G. Young Jr., L. Que Jr., *Angew. Chem. Int. Ed. Engl.* **35**, 618 (1996).
37. K. Kim and S. J. Lippard, *J. Am. Chem. Soc.* **118**, 4914 (1996).
38. P. R. Ortiz de Montellano, Ed., *Cytochrome P-450: Structure, Mechanism, and Biochemistry* (Plenum, New York, 1986).
39. J. H. Dawson, *Science* **240**, 433 (1988) and references therein.
40. R. C. Scarrow *et al.*, *J. Am. Chem. Soc.* **109**, 7857 (1987).
41. Supported by NSF grant MCB-9405723 (L.Q.), NIH grants GM-40466 (J.D.L.) and GM-22701 (E.M.), a University of Minnesota Graduate School Doctoral Dissertation Fellowship (L.S.), and an NIH Predoctoral Traineeship (J.C.N., GM-08277). Beamline X9B at the NSLS was supported by NIH grant RR-001633. We thank M. Chance and E. Sheuring at NSLS Beamline X9B for technical guidance.

8 October 1996; accepted 27 November 1996

Detection and Characterization of the Cumulene Carbenes H_2C_5 and H_2C_6

M. C. McCarthy,* M. J. Travers, A. Kovács, Wei Chen, Stewart E. Novick, C. A. Gottlieb, P. Thaddeus

Two cumulene carbenes, H_2C_5 and H_2C_6, were detected in a supersonic molecular beam by Fourier transform microwave spectroscopy. Their rotational and leading centrifugal distortion constants were determined with high accuracy, such that the entire radio spectrum can now be calculated. Like the known carbenes H_2C_3 and H_2C_4, both molecules have singlet electronic ground states and linear carbon-chain backbones. They can be produced in sufficiently high concentrations in the laboratory that their electronic spectra, expected to lie in the visible, should be readily detectable by laser spectroscopy. The microwave spectra of other, more exotic isomers may be detectable as well.

Carbenes are highly reactive organic molecules with two nonbonded electrons localized on a single C atom. They are important intermediates in terrestrial chemistry, and several have now been detected in the interstellar gas or in circumstellar shells (*1*). Of particular interest in both combustion processes and astrochemistry are the cumulene carbene chains $H_2C=(C=)_nC:$, which may be important building blocks in the syntheses of long hydrocarbons and pure C chains implicated in the formation of fullerenes (*2*). Like organic dyes, cumulene carbenes are likely to have intense optical electronic transitions, which may provide a powerful and convenient way to monitor combustion processes, and they are promising candidates for carriers of the interstellar optical diffuse bands, the identification of which constitutes one of the outstanding unsolved problems in astronomical spectroscopy (*3*). Gas phase studies that establish the geometric and electronic structure of such C chain carbenes are essential if we are to understand their chemical reactivities (*4*), but few have been studied spectroscopically because of their high reactivity. Although we have recently detected long hydrocarbon radicals and closed shell cyanopolyynes (for example, $C_{11}H$ and $HC_{13}N$), the longest cumulene carbene known to date is H_2CCCC (*5*).

By using Fourier transform microwave (FTM) spectroscopy (*6*) of a supersonic molecular beam (Fig. 1), we have now detected the next two members of the cumulene carbene sequence, H_2C_5 ($H_2C=C=C=C=C:$, pentatetraenylidene) and H_2C_6 ($H_2C=C=C=C=C=C:$, hexapentaenylidene). Nine *a*-type *R*-branch ($\Delta J = 1$, where J is the rotational angular momentum quantum number) transitions of H_2C_5 and 13 transitions of H_2C_6 were measured in the frequency range from 8 to 23 GHz. In both molecules, the rotational transitions are grouped into fairly tight triplets with an intensity ratio of approximately 3:2:3 and a splitting of about ±0.1% of the frequency (for example, ±17 MHz at 13.4 GHz for H_2C_6). The relative intensities are those expected at low temperature for a slightly asymmetric top with two equivalent H atoms, and the splitting is in quantitative agreement with that calculated by scaling from the rotational constants of H_2C_3 (*7*) and H_2C_4 (*5*). Because of ortho-para spin statistics, rotational levels where K (the projection of the rotational angular momentum on the C_2 symmetry axis) is ±1, which lie about 14 K above the $K = 0$ levels in both carbenes (Fig. 2), are metastable. Therefore, they are populated in our molecular beam even though the rotational temperature is only about 3 K.

We determined spectroscopic constants by fitting a theoretical spectrum calculated from a standard asymmetric top Hamiltonian (*8*) to the observed frequencies. Two rotational constants (B and C) and two centrifugal distortion constants (D_J and D_{JK}) were obtained for each carbene (Table 1). Transition frequencies ($\nu_{J\leftarrow J-1}$) for the $K = 0$ and the two $K = \pm 1$ ladders of each can be calculated from the approximate expression

Table 1. Spectroscopic constants of H_2C_5 and H_2C_6 (in megahertz). These rotational and centrifugal distortion constants are from a least squares fit of Watson's *S*-reduced Hamiltonian. The root mean square (3 kHz) of the fits is comparable to the measurement uncertainties. Uncertainties (1σ) are in units of the last significant digit.

Constant	H_2C_5		H_2C_6	
	Laboratory	Expected*	Laboratory	Expected*
A	277,600†	287,600	268,400†	286,100
B	2,304.7844(3)	2,304(5)	1,348.0891(1)	1,345(2)
C	2,285.8053(3)	2,285(5)	1,341.3519(1)	1,341(2)
$D_J \times 10^3$	0.104(6)	0.088‡	0.0283(12)	0.0353§
D_{JK}	0.0464(2)		0.0164(1)	

*From (*10*). †Derived assuming a planar structure, that is, $1/C - 1/A - 1/B = 0$. ‡From (*27*). §From (*28*).

M. C. McCarthy, M. J. Travers, P. Thaddeus, Division of Engineering and Applied Sciences, Harvard University, 29 Oxford Street, Cambridge, MA 02138, USA, and Harvard-Smithsonian Center for Astrophysics, 60 Garden Street, Cambridge, MA 02138, USA.
A. Kovács and C. A. Gottlieb, Division of Engineering and Applied Sciences, Harvard University, 29 Oxford Street, Cambridge, MA 02138, USA.
W. Chen and S. E. Novick, Department of Chemistry, Wesleyan University, Middletown, CT 06459, USA.
*To whom correspondence should be addressed.